Biomaterials xxx (2013) 1–9

Contents lists available at ScienceDirect

Biomaterials

journal homepage: www.elsevier.com/locate/biomaterials

# Targeted detection of phosphatidylserine in biomimetic membranes and *in vitro* cell systems using annexin V-containing cubosomes

Hsin-Hui Shen [a,b,*], Vanessa Lake [c], Anton P. Le Brun [c], Michael James [d,e], Anthony P. Duff [c], Yong Peng [a], Keith M. McLean [a], Patrick G. Hartley [a]

[a] *Materials Science and Engineering, CSIRO, Bayview Avenue, Clayton, VIC 3168, Australia*
[b] *Department of Biochemistry and Molecular Biology, Monash University, Clayton, VIC 3168, Australia*
[c] *The Bragg Institute, Australian Nuclear Science and Technology Organization (ANSTO), New Illawarra Rd, Lucas Heights, NSW 2234, Australia*
[d] *The Australian Synchrotron, 800 Blackburn Rd, Clayton, VIC 3168, Australia*
[e] *School of Chemistry, University of New South Wales, Kensington, NSW 2052, Australia*

ARTICLE INFO

*Article history:*
Received 12 June 2013
Accepted 11 July 2013
Available online xxx

*Keywords:*
Apoptosis
Biosensor
Confocal microscopy
Lipid
Liquid crystal
Surface analysis

ABSTRACT

In this work we have formulated Annexin V (ANX) decorated phosphatidylserine containing phytantriol (PSPhy) cubosomes to act as probes for the enhanced detection of apoptotic membranes in both model and *in vitro* cell systems. Small angle X-ray scattering (SAXS) and cryogenic-transmission electron microscopy (Cryo-TEM) indicated that ANX-containing PSPhy (ANX-PSPhy) cubosomes retain the Pn3m cubic symmetry and cubic phase nanoparticle characteristics of PSPhy cubosomes. The interaction of ANX-PSPhy cubosomes with apoptotic model and cellular membranes was also investigated using both quartz crystal microbalance with dissipation and confocal microscopy which confirmed that ANX-PSPhy cubosomes can selectively bind to apoptotic cells and model membranes. Neutron reflectometry has also been used to show strong binding of ANX-PSPhy cubosomes to a model apoptotic membrane, and in addition reveals changes in both the bilayer structure and in the internal structure of the cubosome in a region adjacent to the membrane as a result of material exchange. This material exchange between cubosome and apoptotic model bilayer was further demonstrated using Cryo-TEM. We have demonstrated that lipid bound protein, in this case Annexin V, can be used to target cubosome systems to biological surfaces *in vitro*.



## 1. Introduction

Phosphatidylsereine (PS) is one of the most abundant anionic lipids in the plasma membrane of eukaryotic cells and is, under most conditions, confined to the cytoplasmic side of the membrane. Under certain circumstances, for instance during apoptosis, (programmed cell death) the PS is translocated to the outer side of the membrane. As a consequence methods to detect and image PS on the cell membrane have been developed using targeting molecules, the most common, of which is the 35 kDa protein Annexin V (ANX) [1–4]. Earlier studies have confirmed that ANX selectively binds to PS containing vesicles, supported lipid bilayers and cell membranes [5–8]. These properties have resulted in the development of diagnostic tools based on ANX for the detection of apoptosis *in vivo* using radiological and microscopic fluorescent techniques [9,10]. Annexin V has a number of drawbacks for PS imaging which include its size, stability, high cost and the need for the presence of calcium ions to enable binding. [5].

Bicontinuous cubic lyotropic liquid-crystalline phases are nanostructured, self-assembled systems based on surfactants and lipids. Their amphiphilic components allow them to solubilize hydrophilic, hydrophobic and other amphiphilic species, and they have found applications in delivery within the pharmaceutical [11–15], food [16,17] and cosmetics [18] industries. Phytantriol (3, 7, 11, 15-tetramethylhexadecane-1, 2, 3-triol, (Phy)) is a commonly used surfactant which displays a bicontinuous cubic phase, comprising 15% water under physiological conditions [19,20]. Importantly, an equilibrium is found between the cubic phase and excess water, which provides the necessary conditions for the dispersion of the cubic phase into colloidal formulations, known as cubosomes.

Recently, we co-formulated phytantriol (Phy) with the naturally occurring negatively charged membrane lipid, di-palmitoylphosphatidylserine (DPPS) to produce DPPS-containing phytantriol

* Corresponding author. Materials Science and Engineering, CSIRO, Level 2, Building 76, Room 237, Bayview Avenue, Clayton, VIC 3168, Australia. Tel.: +61 3 95458108; fax: +61 3 95458106.
*E-mail addresses:* hsin-hui.shen@monash.edu, hsin-hui.shen@univ.oxon.org (H.-H. Shen).

0142-9612/$ – see front matter © 2013 Elsevier Ltd. All rights reserved.
http://dx.doi.org/10.1016/j.biomaterials.2013.07.042

dispersions (PSPhy) [21]. Nanostructural phase transitions due to increasing DPPS content were correlated with increases in cellular uptake and cytotoxicity. Further investigations of the interaction of these cubosomes with supported lipid bilayers were made using neutron reflectometry (NR) [22] which revealed that lipid exchange and structural rearrangements occurred for both Phy and PSPhy cubosomes. PSPhy cubosomes showed a greater ability than pure Phy cubosomes to penetrate the cell membrane via a membrane fusion mechanism. In this study we present a study of the binding of ANX to fluorescently labelled PSPhy cubosomes and explore their utility to reduce ANX usage while enhancing the fluorescence signal when targeting phosphatidylserine-containing model membranes and apoptotic HeLa cells *in vitro*. We have employed SAXS and Cryo-TEM to characterize the nanostructure of these systems. Quartz crystal microgravimetry has been used to simulate and study membrane attachment processes using a model supported lipid bilayer system. Detailed structural information associated with the interaction between ANX-PSPhy cubosomes and apoptotic model membranes was obtained using neutron reflectometry (NR). We have produced both protonated and partially deuterated ANX to functionalize PSPhy cubosomes which allows us to determine these complex adsorbed structures when used in conjunction with protonated and deuterated supported lipid bilayers and multiple solution contrasts. Confocal microscopy has been used to detect fluorescently labelled ANX-PSPhy cubosome attachment, uptake and ultimate cytotoxicity towards both healthy and apoptotic HeLa cells as a model system *in vitro*.

## 2. Materials and methods

### 2.1. Materials

Commercial grade phytantriol (Phy, 98.0%, 1,2,3-trihydroxy-3,7,11,15-tetramethylhexadecane) was obtained from DSM Nutritional Products. Pluronic F127 (Poly(ethylene oxide)-poly(propyleneoxide)-poly(ethylene oxide) (PEO-PPO-PEO)), was purchased from BASF (Melbourne, Australia). 1,2-dihexadecanoyl-sn-glycero-3-phospho-L-serine (DPPS, sodium salt) was purchased from Genzyme Pharmaceuticals Australasia (Sydney, Australia). Non-deuterated and palmitoyl chain deuterated 1-palmitoyl-2-oleoyl-*sn*-glycero-3-phosphocholine (POPC) and non-deuterated1-palmitoyl-2-oleoyl-*sn*-glycero-3-phospho-L-serine (sodium salt) (POPS) were purchased from Avanti Polar Lipids Inc. (Alabaster, AL, USA). These chemicals were used as received without further purification. Polished silicon blocks were purchased from Crystran Ltd (Poole, Dorset, UK).

### 2.2. Production of annexin V protein

Protonated and partially deuterated forms of the Annexin V protein were produced at the National Deuteration Facility at the Australian Nuclear Science and Technology Organisation.

#### 2.2.1. Generation of pET28a_Annexin V expression construct

The construct pPROEX-Htb_AxV encoding the human Annexin V protein (Accession no. NP_001145) was kindly donated by Prof. Seamus J. Martin (Trinity College, Dublin, Ireland) [23]. The Annexin V gene was sub-cloned from this construct into pET28a (Novagen). A PCR fragment with 5′-NdeI and 3′-HindIII restriction sites was generated using the pPROEX-Htb_AxV construct as template and the primers: 5′-GCCATATGGCACAGGTTCTCAGAGGCACT-3′ (forward primer including underlined NdeI site) and 5′-GCAAGCTTAGTCATCTTCTCCACAGAGCAGCAG-3′ (reverse primer including the underlined HindIII site). The PCR conditions used were: 30 s at 98 °C; 10 s at 98 °C, 20 s at 62 °C, 20 s at 72 °C for 30 cycles and 10 min at 72 °C. The amplified Annexin V gene was subsequently digested with NdeI and HindIII and ligated into pET28a. The resulting recombinant plasmid was sequenced and named pET28a_AxV. This construct produces a full-length Annexin V protein with a thrombin-cleavable N-terminal $His_6$ tag with the sequence; **HHHHHH***SSGLVPRGSH*M, with the $His_6$ tag in bold, the thrombin cleavage site in italics and the start methionine of Annexin V underlined.

#### 2.2.2. Growth media used in the expression of annexin V

All growth of *Escherichia coli* was carried-out in ModC1, a modified version of the C1 minimal media described in Middelberg et al. [24]: 40 g $L^{-1}$ glycerol, 4.16 g $L^{-1}$ $Na_2HPO_4$, 2.58 g $L^{-1}$ $NH_4Cl$, 2.54 g $L^{-1}$ $KH_2PO_4$, 1.94 g $L^{-1}$ $K_2SO_4$, 0.33 g $L^{-1}$ $MgSO_4$, 0.1 g $L^{-1}$ sodium citrate, 4.8 mg $L^{-1}$ Thiamine-HCl, 0.91 mg $L^{-1}$ $FeCl_2$, 0.49 mg $L^{-1}$ $CuSO_4$, 0.44 mg $L^{-1}$ $MnCl_2$ and 0.41 mg $L^{-1}$ $ZnCl_2$. For the partial deuteration of Annexin V, deuterated ModC1 (d-ModC1) media was used. This was made with 100% $D_2O$ and all hydrogenated constituents. The expression levels of Annexin V in both hydrogenated and deuterated ModC1 media was tested on small-scale prior to large-scale deuterated growth (Supplemental Fig. S1).

#### 2.2.3. Large-scale over-expression of hydrogenated and partially deuterated annexin

For the growth of *E. coli* in ModC1 and d-ModC1 and expression of Annexin V the procedure by Chen et al. [25] was followed. Competent *E. coli* BL21(DE3)star (Invitrogen) cells were freshly transformed with the pET28a_AxV expression construct and grown in 30 mL of either ModC1 or d-ModC1 (supplemented with 40 μg/mL of Kanamycin) overnight in a shaking incubator (250 rpm) at 37 °C. After 20 h of growth, the starter culture was used to inoculate 1 L of either ModC1 or d-ModC1 media in a 2 L bioreactor vessel. For the hydrogenated growth, the starting $OD_{600nm}$ was 0.055 and biomass was generated for 23 h to an $OD_{600nm}$ of 14. At this point, the culture was induced with 1 mM IPTG and left to grow for a further 17 h, until the carbon source was exhausted, at which point the biomass was harvested. The final $OD_{600nm}$ for this culture was 35. For the deuterated growth, the starting $OD_{600nm}$ was 0.075 and biomass was generated for 44 h to an $OD_{600nm}$ of 16. At this point, the culture was induced with 1 mM IPTG and left to grow for a further 21 h, until the carbon source was exhausted, at which point the biomass was harvested. The final $OD_{600nm}$ for this culture was 27.4. Cells were collected and centrifuged at 8000× g for 30 min at 4 °C. The cell pellets were stored at −80 °C until purification.

#### 2.2.4. Purification of hydrogenated and partially deuterated recombinant annexin V

Cell pellets were resuspended in 200 mL of lysis buffer (50 mM $NaH_2PO_4$, 300 mM NaCl, 10 mM Imidazole, 1 mg/mL lysozyme) and incubated on ice for 30 min. Cells were then disrupted by sonication, on ice, using six 30 s pulses of 40 W (with 30 s pauses between pulses). Insoluble material was then removed by centrifugation at 45,000× g for 30 min at 4 °C. The supernatant was retained on ice and then loaded onto a 5 mL HisTrap FF column (GE Healthcare) which had been equilibrated with 25 mL of wash buffer (50 mM $NaH_2PO_4$, 300 mM NaCl, 20 mM Imidazole). The column (with bound His-tagged Annexin V) was washed with 50 mL of wash buffer. Annexin V was then eluted with 8 mL of elution buffer (50 mM $NaH_2PO_4$, 300 mM NaCl, 250 mM Imidazole). The fractions containing Annexin V were pooled and run through a HiLoad 16/60 Superdex 75 pg column (GE Healthcare) pre-equilibrated with Annexin V storage buffer (40 mM Tris−HCl pH 7.5, 150 mM NaCl, 1 mM DTT, 0.05% sodium azide) to further remove any retained impurities. Both purified hydrogenated and partially deuterated recombinant Annexin are analysed by SDS PAGE (Supplemental, Fig. S2). Furthermore the final deuteration of deuterated recombinant Annexin V is around 82 ± 1% according to the MALDI-TOF spectroscopy data (Supplemental Fig. S3). Fractions containing Annexin V were pooled and aliquots were stored at −80 °C.

### 2.3. Preparation of cubosome formulations

2.3 wt% DPPS - 90.7 wt% Phy/7 wt% F-127/water (PSPhy) cubosomes were prepared by weighing 150 mg of phytantriol and 3.75 mg of DPPS into a 20 mL glass vial and adding 0.5 mL of a solution of pluronic F127 dispersant in chloroform (22.6 mg/mL). The mixtures were vortex-mixed thoroughly and then placed in a rotary evaporator for 2 h and freeze-dried to remove the chloroform. 15 mL of Milli-Q water was added prior to dispersion by ultrasonication (MisonixXL2000, Misonix Incorporated) for 10 min in pulse mode (5 s pulses interrupted by 5 s breaks) at 75% of maximum power, resulting in a milky dispersion (PSPhy cubosomes). ANX-PSPhy cubosomes were prepared by incubating ANX with PSPhy cubosomes solution (1 mg/mL) at a ratio of 1:20 in 10 mM HEPES buffer at pH 7.5 solution with 2.5 mM $CaCl_2$ for 10 min before the experiments.

The quaternary structure of the mixtures was investigated using a sodium dodecyl sulphate polyacrylamide gel electrophoresis (SDS-PAGE) assay, which enabled us to separate proteins according to their size. PSPhy cubosomes were incubated with ANX for 1 h in a solution of 10 mM HEPES buffer at pH 7.5, with 2.5 mM $CaCl_2$ followed by the addition of an equal volume of ×2 gel loading buffer. The protein samples were then heated to 95 °C for 3 min prior to loading onto a 12% SDS-PAGE gel.

### 2.4. Cell culture and cell viability tests

Cell viability tests were conducted using HeLa cells. The cells were plated in 96-well polystyrene cell culture plates at a density of $5 \times 10^3$ cells per well and allowed to attach to the well surface for 24 h. If required, HeLa cells were induced to undergo apoptosis by treatment with staurosporine (STS, 1 μM final concentration) for 8 h, followed by rinsing with cell culture medium 3 times before adding samples. 20 μg/mL of PSPhy cubosomes in cell culture medium were filtered through a 0.2 μm Acrodisc® syringe filter prior to mixing with ANX in HEPES-2.5 mM $CaCl_2$ buffer and subsequently added to the wells. Cell viability was also examined using a MTT [3-(4,5-Dimethylthiazol-2-yl)-2,5-diphenyltetrazolium bromide (tetrazole)] assay [26]. In the presence of viable cells, MTT is reduced resulting in precipitation of water-insoluble, purple formazan within the cells. Dimethyl sulfoxide was added to dissolve the insoluble formazan into a coloured solution and an UV−visible

Please cite this article in press as: Shen H-H, et al., Targeted detection of phosphatidylserine in biomimetic membranes and *in vitro* cell systems using annexin V-containing cubosomes, Biomaterials (2013), http://dx.doi.org/10.1016/j.biomaterials.2013.07.042

spectrometer (BioTek Microplate Reader) utilised to measure the absorbance of the solution at 570 nm.

### 2.5. Cellular uptake of cubosomes using confocal microscopy

HeLa cells were transfected with CellLight™ plasma membrane green fluorescent protein (PM-GFP) purchased from Invitrogen and the manufacturer's standard protocol was followed to express the GFP on the plasma membrane. 200 μL of 200 μg/mL ANX-functionalized octadecyl rhodamine B chloride (R18)-labelled PSPhy cubosomes was added to 1.8 mL cell culture medium in a FluoroDish™ for live cell imaging. The PM-GFP HeLa cells were imaged directly under cell culture conditions, 24 h after cubosome addition.

### 2.6. Vesicle formation

2:1 (by weight) POPC:POPS in chloroform were dried under a gentle stream of nitrogen and then freeze dried overnight to remove any residual chloroform. To prepare large multilamellar vesicles, phospholipids were first suspended in a HEPES buffer solution to give a lipid concentration of 1 mg/mL, followed by vortexing the tube vigorously to completely re-suspend the phospholipid. This results in a milky, uniform suspension which was then sonicated to break it into small unilamellar vesicles (SUV) using a tip probe sonicator in an ice water bath maintained at 4 °C. Typical sonication times of 10–30 min were required for the suspension to change from milky to nearly clear (i.e., only very slightly hazy) in appearance. The suspension of SUV was then diluted to give a final concentration of 0.1 mg/mL in HEPES buffer. The SUV solutions were centrifuged at a low speed for 30 min at 4 °C to remove traces of titanium particles which were released by the sonicator tip.

### 2.7. Neutron reflectometry (NR)

NR data were collected using the Platypus time-of-flight neutron reflectometer at the OPAL 20 MW research reactor (Australian Nuclear Science and Technology Organisation (ANSTO), Sydney, Australia) [27,28]. 23 Hz cold neutron pulses of bandwidth 2.8 Å $\leq \lambda \leq$ 18.0 Å were generated using a disc chopper system (EADS Astrium GmbH) in low resolution mode ($\Delta\lambda/\lambda = 7\%$), and the direct and reflected beam spectra recorded on a 2-dimensional helium-3 neutron detector (Denex GmbH). Measurements were undertaken at 37 °C by using thermostatically controlled water flowing through top- and base-plates of the solid–liquid cells. Reflected beam spectra for the POPC/POPS bilayer only data were collected at $\theta_1 = 0.7°$ for 1 h and at $\theta_2 = 3.2°$ for 3 h. Reflected beam data following the addition of cubosomes, used reduced data collection times (0.25 h for $\theta_1$ and 1.25 h for $\theta_2$). Constant illumination of the sample was achieved using collimating slits set at 30 mm wide × 0.7 mm high for $\theta_1$, and 30 mm wide × 3.2 mm high for $\theta_2$. Direct beam measurements were collected in transmission through the Si blocks under the same collimation conditions for 1 h each. When the Platypus data was reduced using the SLIM reduction package [29], the resolution function was automatically calculated and used in the model fitting. Analysis of the NR profiles was performed using the MOTOFIT analysis program [30]. All models included an oxide layer on the surface of the Si substrates followed by a three-layer structure (head group–chain–head group) to represent the scattering length density (ρ) and thickness of the lipid bilayer. A lamellar structure model based on the optical matrix method [31,32] was used to represent the cubosomes on the supported lipid membrane. The membrane-bound cubosomes were modelled using a cubic structure model [33,34] which fits a sinusoidal variation in scattering length density normal to the plane of the surface using the following equation:

$$\rho(z) = \rho_{\text{avaerage}} + A\sin\left[\left(\frac{2\pi z}{l}\right) + \phi\right]$$

Where $\rho_{\text{avaerage}}$ is the average SLD in the sinusoidal region, $A$ is the amplitude of the oscillations, $l$ is the repeat distance, $z$ is the distance from the surface and $\phi$ is the phase of the oscillations.

### 2.8. Cryogenic transmission electron microscopy (Cryo-TEM)

Samples were examined using a Gatan 626 cryoholder (Gatan, Pleasanton, CA, USA) and Tecnai 12 Transmission Electron Microscope (FEI, Eindhoven, The Netherlands) at an operating voltage of 120 kV. At all times low dose procedures were followed, using an electron dose of 8–10 electrons/Å$^2$ for all imaging. Images were recorded using a Megaview III CCD camera and AnalySIS camera control software (Olympus.) using magnifications in the range 30,000× to 97,000×.

### 2.9. Small angle X-ray scattering (SAXS)

The X-ray scattering experiments were performed at 37 °C in 1.0 mm quartz capillaries using the SAXS/WAXS beamline at the Australian Synchrotron. A wavelength of 1.24 Å was employed to record 2D SAXS image patterns using a Pilatus-1M CCD camera. A measurement time of 1 s was employed to minimise beam damage. The scattering of the empty capillary without water was subtracted to give the scattering intensity from the cubosome dispersions. Analysis of the diffraction peaks was performed using the AXcess analysis program.

### 2.10. Quartz crystal microbalance with dissipation monitoring (QCM-D)

QCM-D measurements were performed using a Q-SENSE E4 system equipped with an Axial Flow Chamber using 50 nm silicon oxide sensors. Details of the apparatus are described elsewhere [21,35]. The temperature was held constant at 37 °C during the experiments. Upon adsorption of matter to the surface of a sensor crystal, the change in frequency of the sensor movement ($\Delta f$) reflects the film mass (including coupled water). The damping of the movement ($\Delta D$) correlates to the viscoelastic properties with a time resolution of 1 s. The resonance frequency and the dissipation were measured at several harmonics (15, 25 and 35 MHz) simultaneously.

## 3. Results and discussion

Earlier studies have shown that anionic phospholipid vesicles in the presence of calcium ions induce the formation of SDS-resistant oligomers of Annexin V [36]. We have employed a SDS-PAGE cross-linking experiment to investigate the oligomer state of ANX when associated with PSPhy cubosomes (Fig. 1). Pure PSPhy cubosomes were used as a control experiment (in column 2), with no evidence of protein. Column 3 shows pure ANX in the monomeric state (~35 kDa) in the presence of HEPES-2.5 mM $CaCl_2$ buffer at pH 7.4 as expected. Following incubation of ANX with PSPhy cubosomes under the same buffer conditions and subsequent crosslinking, the SDS-PAGE gel (column 4) shows the presence of both monomeric and dimeric forms of the protein, as deduced from the appearance of a new band at ~75 kDa. These results are consistent with previous observations of ANX behaviour in phospholipid vesicles containing anionic lipids [36–38] and show that ANX has the same oligomerization behaviour in the presence of PSPhy cubosomes.

Cryo-TEM has been widely used to visualize dispersed lyotropic liquid crystalline particles [16,21,39–41] and we have used this technique to visualize the nanostructural information of the PSPhy and ANX-PSPhy cubosomes in HEPES-2.5 mM $CaCl_2$ buffer at pH 7.4. Fig. 2(a) presents a cryo-TEM image of PSPhy cubosomes, and images

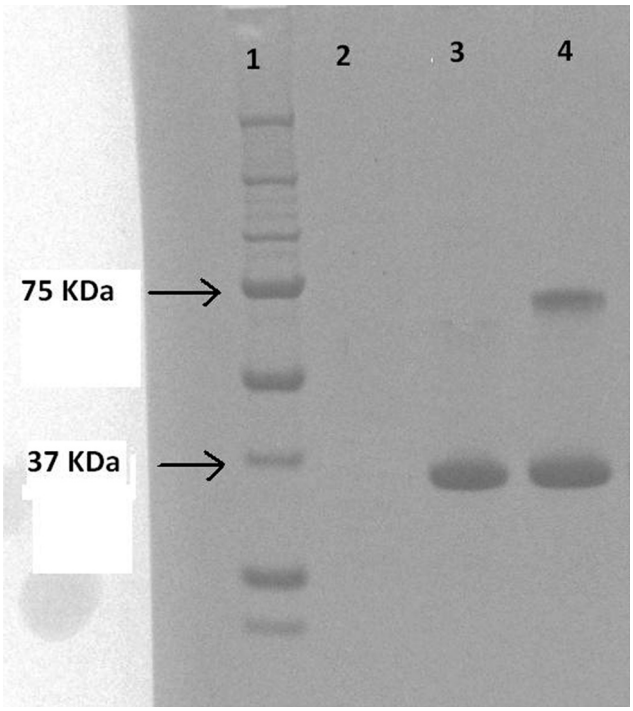


**Fig. 1.** SDS PAGE gel of: Lane 1. Protein molecular weight markers (Mark 12, Invitrogen), Lane 2. PSPhy cubosomes, Lane 3. ANX, Lane 4. ANX-PSPhy cubosomes.

Please cite this article in press as: Shen H-H, et al., Targeted detection of phosphatidylserine in biomimetic membranes and *in vitro* cell systems using annexin V-containing cubosomes, Biomaterials (2013), http://dx.doi.org/10.1016/j.biomaterials.2013.07.042

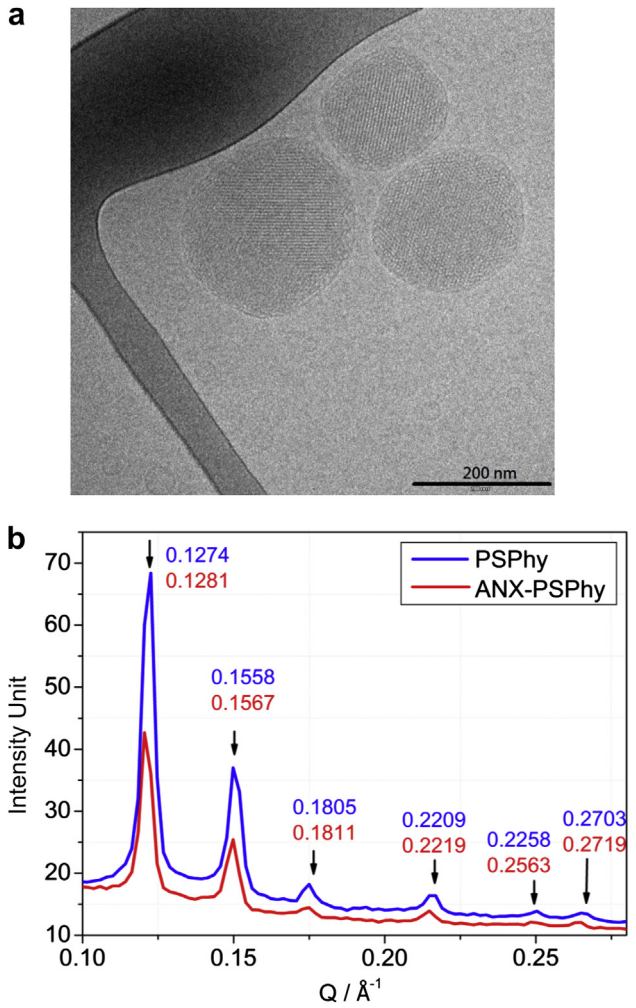


**Fig. 2.** (a). Cryo-TEM images of PSPhy cubosomes and (b). Synchrotron SAXS profiles showing the scattering profiles of the PSPhy cubosomes (blue) and ANX-PSPhy cubosomes in HEPES-2.5 mM $CaCl_2$ buffer at 37 °C. (For interpretation of the references to colour in this figure legend, the reader is referred to the web version of this article.)

of ANX-PSPhy cubosomes are essentially the same (Supplemental Fig. S4). The Cryo-TEM image shows cubosome nanoparticles ranging from 50 nm to 250 nm in diameter, with an internal periodicity of electron density typical of cubic phase materials [21].

In order to gain further insights into the nanostructural changes resulting from ANX addition, we have used synchrotron-based SAXS to characterize the internal cubic phase symmetry of the dispersed particles. The SAXS scattering curves for the aqueous dispersions with and without ANX in the presence of PSPhy cubosomes were obtained at 37 °C under the same buffer condition as for the Cryo-TEM measurements (Fig. 2(b)). The Bragg peaks in these scattering profiles indicate that both the PSPhy and ANX-PSPhy cubosomes have the characteristic spacing of a crystalline cubic lattice of Pn3m symmetry (double diamond). The peaks can be indexed using the following Miller indices {1,1,0}, {1,1,1}, {2,0,0}, {2,1,1}, {2,2,0} and {2,2,1} [40], and yields lattice parameters of around 69 Å for both samples, which are consistent with other measurements in the literature [21,41]. There is very little shift in the Bragg peak positions of the ANX-PSPhy cubosomes relative to non ANX containing PSPhy cubosomes, indicating that the presence of protein has negligible effect in the liquid crystalline structure. Furthermore, these SAXS data indicate that there is no manifest structural transition associated with the binding of ANX to the PSPhy cubosomes. A previous study by Conn et al. [42] has shown that phytantriol cubosomes undergo a substantial change in their internal structure upon incorporation of an integral membrane protein, the dopamine D2L receptor. Not only was a 28% increase in the lattice parameter observed (expanding to 97 Å), but in addition, structural phase transitions upon heating were modified by the presence of D2L. The increased lattice parameter in their study clearly indicates protein loading inside the phytantriol cubic phase structure.

Cryo-TEM and SAXS data showed that there is no nanostructural phase transition of PSPhy cubosomes with the addition of ANX. Therefore ANX is presumably only associated with the surface of PSPhy cubosomes. To probe the availability of the surface associated ANX, a model apoptotic cell membrane consisting of 1-palmitoyl-2-oleoyl-*sn*-glycero-3-phosphocholine (POPC)/1-palmitoyl-2-oleoyl-*sn*-glycero-3-phospho-L-serine (sodium salt) (POPS) at the ratio of 2:1 (w:w) was prepared as a supported bilayer on a QCM-D crystal using the vesicle rupture method. We then examined the interaction of ANX-PSPhy cubosomes with the supported model apoptotic cell membrane. Fig. 3 shows the QCM-D response for the POPC/POPS vesicles interacting with the $SiO_2$-coated QCM sensor surface. Vesicles first adsorb, and then when a sufficiently high surface coverage is reached (~1¼ hrs), they transform spontaneously to a bilayer after rinsing with HEPES buffer containing 10 mM $CaCl_2$. Following bilayer formation, the cell was rinsed with HEPES buffer with 2.5 mM $CaCl_2$ at pH 7.4. This is introduced to equilibrate with the bilayer, providing the same solution conditions as present in the next ANX-PSPhy cubosomes addition. The frequency change of ~22 Hz resulting from bilayer formation is complete 2.8 h after the initial injection and is consistent with earlier studies [43–45], and the change of $CaCl_2$ did not affect the frequency change of the final bilayer. The decrease in frequency of 3rd and 5th overtones is the same (as is the dissipation response), suggesting that the bilayer is effectively rigid, and therefore that the Saurbrey equation can be used to determine the adsorbed mass [46]. This results in a mass of 360 ng/cm$^2$ for the POPC/POPS (2:1 w:w), bilayer, which is typical for a supported lipid bilayer on a $SiO_2$ surface. [21,43,44].

Fig. 3 also shows the QCM response following addition (at 2.8 h) of 0.1 mg/mL ANX-PSPhy cubosomes (in HEPES-2.5 mM $CaCl_2$ buffer at pH 7.4) to the supported POPC/POPS bilayer. This results in a drop in the frequency (blue squares, $\Delta f(5) = -90$ Hz), indicating mass uptake at the POPC/POPS bilayer surface. Moreover, there is a

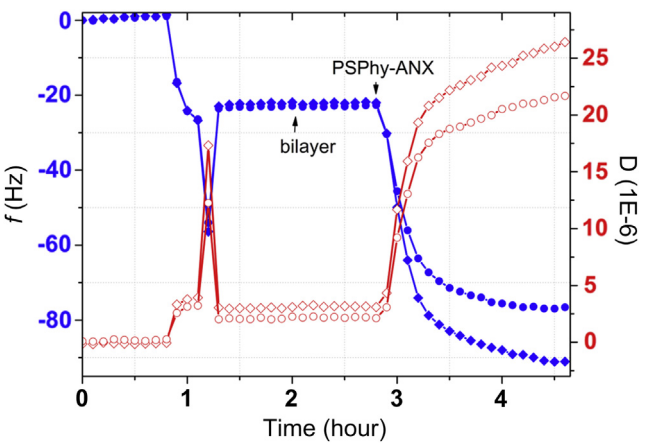


**Fig. 3.** QCM-D measurements of the interaction of ANX-PSPhy cubosomes with a POPC/POPS (2:1, w:w) bilayer. $f(3)$:blue circles, $f(5)$: blue square, $D(3)$:open red circle and $D(5)$:, open red square. (For interpretation of the references to colour in this figure legend, the reader is referred to the web version of this article.)

Please cite this article in press as: Shen H-H, et al., Targeted detection of phosphatidylserine in biomimetic membranes and *in vitro* cell systems using annexin V-containing cubosomes, Biomaterials (2013), http://dx.doi.org/10.1016/j.biomaterials.2013.07.042

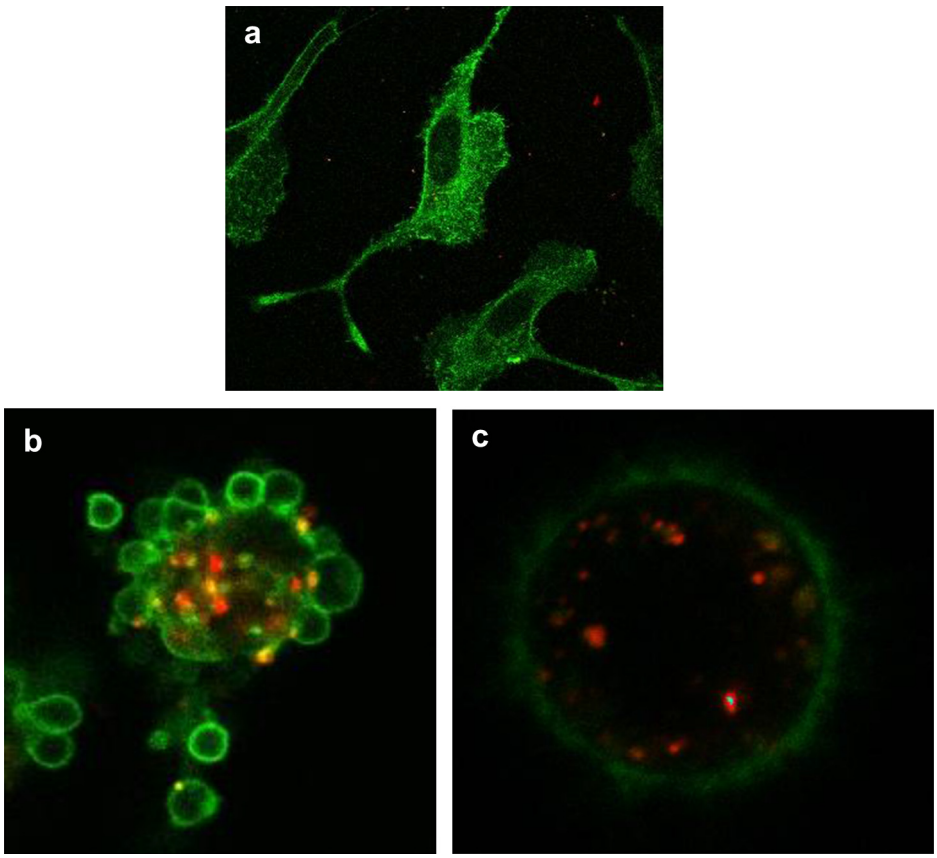


**Fig. 4.** Interaction of the rhodamine labelled ANX-PSPhy cubosomes (red) with HeLa cells stain with PM-GFP (green). (a). Non-apoptotic HeLa cells. (b). Apoptotic HeLa cells (treated with STS). (c) Another controlled experiment while ANX containing fluorescein isothiocyanate (FITC) and PSPhy cubosomes remain red. (For interpretation of the references to colour in this figure legend, the reader is referred to the web version of this article.)

significant divergence of the frequencies of the 3rd and 5th overtones and an increase in dissipation response (blue circles, $\Delta D(5) = 27 \times 10^{-6}$ a.u.), indicating that the bound mass is non-rigid in nature. This is explained by cubosome binding at the bilayer interface as previously described [22]. In this instance, the Sauerbrey equation is not able to correctly estimate the adsorbed mass. Fig. S5(a) (Supporting Information) demonstrates that there is no mass uptake due to ANX-PSPhy cubosomes by a non-POPS containing POPC model membrane, suggesting that the apoptotic mimicking POPS lipid is required for ANX-PSPhy cubosome binding. Similarly, Fig. S5(b) (Supporting Information) reveals that ANX free PSPhy cubosomes do not bind to the POPC/POPS bilayer, indicating that the specific interaction between ANX and POPS is the cause of cubosome binding at the model apoptotic membrane surface.

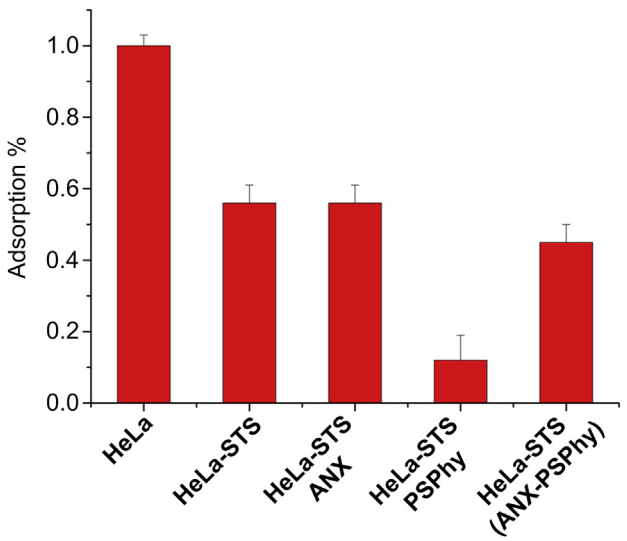


**Fig. 5.** Adsorbtion intensities at 570 nm of healthy HeLa (adsorbtion = 1) and apoptotic HeLa (HeLa-STS) cells incubated in the presence of ANX, PSPhy cubosomes and ANX-PSPhy cubosomes after 24 h of incubation. Cell viability measurements are given relative to those of control samples (HeLa cells only).

We have extended this study to examine the interactions of the cubosomes with normal and staurosporine (STS) [47] induced apoptotic HeLa cells *in vitro* using confocal fluorescence microscopy. HeLa cells transfected with plasma-membrane green fluorescent protein (PM-GFP) and cubosomes containing octadecyl rhodamine B chloride (as a fluorescent marker) were used to evaluate cell–cubosome interactions. Results of incubation of ANX-PSPhy cubosomes at a final concentration of 20 μg/mL with normal and apoptotic HeLa cells after 24 h are shown in Fig. 4. Negligible cubosome fluorescence (rhodamine, red) is observed associated with the non-apoptotic HeLa cells, indicating that there is no binding of cubosomes (Fig. 4(a)). Apoptotic HeLa cells (Fig. 4(b)) however show high levels of rhodamine fluorescence (red dots) at the cell surface; suggesting that ANX-PSPhy cubosomes specifically bind to the apoptotic cell membrane. Yellow fluorescence in Fig. 4(b) results from the colocalization of rhodamine labelled (red) cubosome lipid and the PM-GFP labelled (green) plasma membrane lipid. To demonstrate the enhanced sensitivity of the fluorescent cubosome-ANX conjugate, we loaded PSPhy cubosomes with FITC

Please cite this article in press as: Shen H-H, et al., Targeted detection of phosphatidylserine in biomimetic membranes and *in vitro* cell systems using annexin V-containing cubosomes, Biomaterials (2013), http://dx.doi.org/10.1016/j.biomaterials.2013.07.042

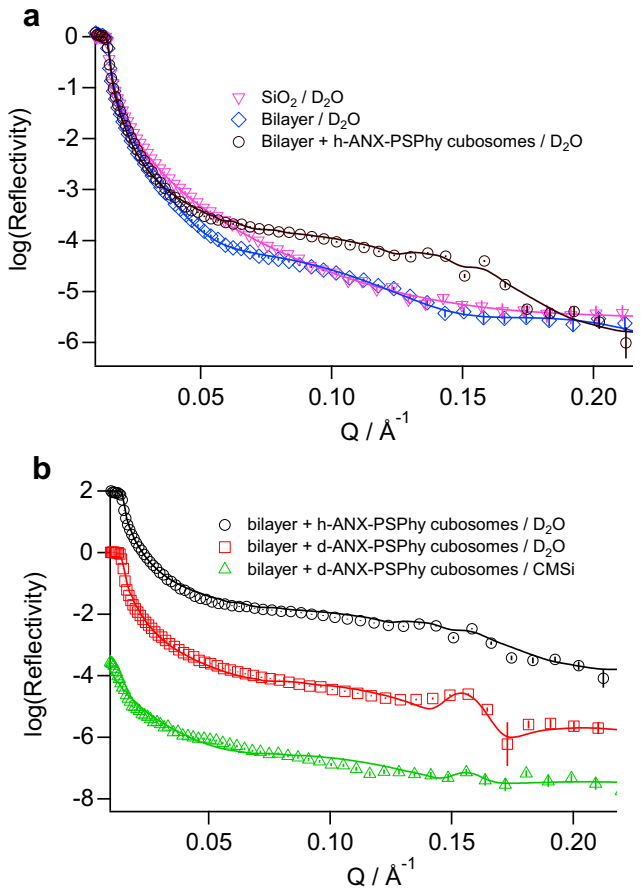


**Fig. 6.** The reflectivity profiles (symbols) and fits (lines) of a) silicon oxide surface in $D_2O$ (▽), a) $d_{31}$-POPC/$d_{31}$-POPS (2:1) bilayer in $D_2O$ (◇), with h-ANX-PSPhy cubosomes deposited (○), and b) the different contrasts used for the ANX-PSPhy cubosomes consisting of h-ANX in $D_2O$ (○), d-ANX in $D_2O$ (□) and d-ANX in CMSi (△). The reflectivity profiles in b) are offset for clarity.

tagged Annexin, and assessed their ability to detect apoptotic cells *in vitro* using confocal fluorescence microscopy. The results are shown in Fig. 4(c). The image shows clear red fluorescence associated with the surface of the apoptotic cell due to the rhodamine loaded cubosome, but no cyan colour due to the FITC tagged Annexin. This is not surprising given the low loading of annexin relative to that typically used to detect apoptotic cells as described above. We therefore suggest that the fluorescent cubosome-ANX dispersion has application as an apoptosis detection reagent *in vitro* and potentially *in vivo*, as it overcomes the weak and transient fluorescence associated with free ANX-FITC [48].

Both QCM-D and confocal microscopy data have clearly indicated that the ANX-PSPhy cubosomes can be used to detect PS in both model supported lipid membranes and in *in vitro* cell culture. In order to further assess the applicability of ANX-PSPhy cubosomes as apoptosis detection agents, it is important to test their cytotoxicity. ANX, PSPhy cubosomes and ANX-PSPhy cubosomes in the concentration range (20 μg/mL) used in these studies were found to be non-cytotoxic against HeLa cells when assessed using the [3-(4,5-Dimethylthiazol-2-yl)-2,5-diphenyltetrazolium bromide (tetrazole)] (MTT) assay to estimate viable cell numbers. These results were consistent with our earlier study using a L929 fibroblast cell line. [21] Fig. 5 shows MTT assay data recorded following exposure of HeLa cells to the different formulations. The addition of the STS, as an apoptotic inducer, results in a ~50% drop in cell absorbance (i.e., cell viability) according to the MTT assay in column 2, and hence this concentration of STS was used in the subsequent measurements. Exposure of these apoptotic cells to non-annexin conjugated PSPhy cubosomes results in a further drop in absorbance, presumably associated with further reduced cell viability. Exposure to ANX-PSPhy cubosomes resulted in a smaller reduction in cell viability. We hypothesise that this is due to ANX blocking cubosome-cell membrane fusion and uptake interactions which were the subject of our previous study.

In an attempt to further understand the membrane structural rearrangements and interactions between ANX-PSPhy cubosomes and the cell membrane we have carried-out a neutron reflectometry study on supported POPC/POPS model membranes under conditions identical to those used in the earlier QCM-D study. The thickness and roughness of the native oxide layer of the silicon wafer substrate was first measured under $D_2O$-HEPES buffer at pH 7.4 (Fig. 6, pink inverse triangles). Data were fitted and the $SiO_2$ thickness was determined to be $10 \pm 1$ Å with a surface roughness of 4 Å. Two separate POPC/POPS (2:1, w:w) bilayers were subsequently deposited onto silicon oxide substrates using the vesicle collapse method described earlier. To assist in determining the composition of the deposited layer, isotopic contrast between the components was exploited by using lipids with a single perdeuterated palmitoyl chain ($d_{31}$-POPC/$d_{31}$-POPS), which results in high scattering contrast with the hydrogenous components of the ANX protein and PSPhy cubosomes in $D_2O$. A second contrast was also used that utilized the use of the deuterated annexin (dANX). This provides contrast between the hydrogenous PSPhy and the hydrogenous parts of the $d_{31}$-POPC/POPS bilayer. Using the deuterated ANX with a contrast where the subphase nSLD is matched to silicon ($2.07\times10^{-6}$ Å$^{-2}$) will give a low contrast against the PSPhy and bilayer but a high contrast against the ANX providing more structural details on the protein components whereas the $D_2O$ subphase matches out the dANX and highlights the bilayer and PSPhy.

Fig. 6 (blue diamonds) shows the NR profiles of a $d_{31}$-POPC/POPS supported bilayer, produced by exposing the $SiO_2$ surface to vesicles (at a concentration of 0.1 mg/mL) for 1½ hours followed by rinsing with $D_2O$-HEPES-2.5 mM $CaCl_2$ buffer. The reflectivity curve displays a broad Kiessig fringe around $Q \sim 0.1$ Å$^{-1}$, indicating the presence of an adsorbed bilayer with high coverage. To further analyse the bilayers we used the MOTOFIT analysis package to create a detailed model [29]. Due to the difference in nSLD values between the hydrophilic heads and the hydrophobic tails, the bilayer was divided into three discrete layers consisting of headgroups 1 (those closest to the silicon oxide layer), lipid tails and headgroups 2 (those closest to the bulk solution). Table one describes the properties of the bilayer and it is found that the bilayer is in good agreement with those previously published [22,33,49]. The total thickness of the bilayer is 47 Å with a surface coverage of 91% and an area per lipid molecule of 72 Å$^2$ (Table 1) which is consistent with palmitoyl-oleyl phospholipid bilayers in the fluid phase [50].

**Table 1**
Substrate and bilayer properties before ANX-PSPhy cubosome binding.

| Layer | Thickness/Å | nSLD/$\times10^{-6}$ Å$^{-2}$ | Volume fraction | Roughness/Å |
|---|---|---|---|---|
| Silicon | – | 2.07 | – | – |
| Silicon oxide | $10 \pm 2$ | 3.47 | – | 4 |
| Head group 1 | $7 \pm 1$ | $2.06 \pm 0.17$ | $0.94 \pm 0.08$ | 4 |
| Tails | $29 \pm 1$ | $3.29 \pm 0.58$ | $0.91 \pm 0.16$ | 4 |
| Head group 2 | $11 \pm 1$ | $2.15 \pm 0.13$ | $0.92 \pm 0.06$ | 4 |
| Bulk solvent | – | 6.35 | – | 4 |

Please cite this article in press as: Shen H-H, et al., Targeted detection of phosphatidylserine in biomimetic membranes and *in vitro* cell systems using annexin V-containing cubosomes, Biomaterials (2013), http://dx.doi.org/10.1016/j.biomaterials.2013.07.042

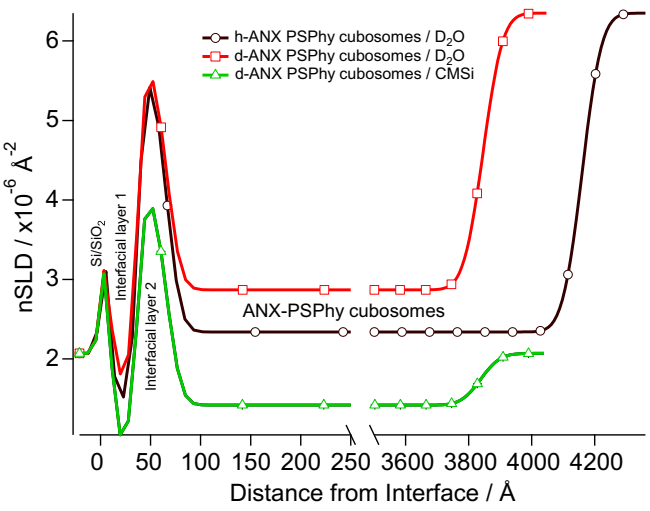


**Fig. 7.** The real space nSLD profile of ANX-PSPhy cubosomes on a bilayer of $d_{31}$-POPC/$d_{31}$-POPS (2:1) in 10 mM Hepes 2.5 mM $CaCl_2$ pH 7.5.

ANX-PSPhy cubosomes at 0.1 mg $mL^{-1}$ were deposited onto the bilayers, incubated for 8 h and the unbound excess removed with a wash of $D_2O$-HEPES buffer. From the h-ANX containing cubosomes (Fig. 6, black circles) it can be clearly seen that the broad fringe at $Q \sim 0.1$ has disappeared at that the specular intensity from $Q > 0.05$ has increased indicating that there is more material present on the surface. Additionally two shallow peaks appear a $Q = 0.14$ $Å^{-1}$ and $Q = 0.16$ $Å^{-1}$ indicating the presence of a nanostructured repeat, consistent with the internal structure of the cubosomes, accumulating at the bilayer interface. When the bilayer is exposed to PSPhy cubosomes containing d-ANX only the peak at $Q = 0.16$ $Å^{-1}$ is observed (Fig. 6, red squares and green triangles).

Previous work has shown that the ANX-PSPhy cubosomes bound to phospholipid bilayers can be modelled using either a lamellar model or a cubic structured model with either model resulting in the same structural description [22,33]. In this work the bilayer-bound ANX-PSPhy cubosomes were analysed using a cubic structure model and used a sinusoidal variation of nSLD along the surface normal (see Materials and Methods for details). From this data analysis it can be clearly noticed that there is perturbation of the bilayer structure (Fig. 7). The bilayer consisting of a three layer model no longer exists. There is now a two layer structure between the silicon oxide surface and the ANX-PSPhy cubosomes. The first layer has a total thickness of 27 Å and has a low nSLD of less than $1.80\times10^{-6}$ $Å^{-2}$ in all contrasts (Table 2). The low nSLD of the layer shows that it mainly consists of PSPhy (76%, Table 2) concentrating at the surface with the remains of the original bilayer (17%). This is an observation that is consistent with other studies that used glycerol monooleate cubosomes and DOPC bilayers which found that only 8% of the original bilayer remained at the silica interface after cubosome addition [49]. To obtain good fits an additional layer between the bilayer remnants and the bulk ANX-PSPhy cubosomes is required. In the $D_2O$ contrasts this layer has a high scattering length density suggesting that there is a high solvent content (Fig. 7 and Table 2). When the subphase is changed to the CMSi contrast in the deuterated ANX case, a high nSLD ($4.20\times10^{-6}$ $Å^{-2}$) is retained suggesting an accumulation of ANX in this layer. The thickness of this layer is 29 ± 6 Å which would be consistent with the thickness of the short axis of the ANX protein of 37 Å from X-ray crystallography data [38].

Adjacent to the second interfacial layer is the nanostructured ANX-PSPhy cubosomes with a total thickness ranging between 3772 Å and 4094 Å. The internal structure of the cubosomes is comprised of between 84 and 92 repeating cubosome units, with repeating internal structures ranging between 41 and 46 Å (Table 2). The properties for each cubosome layer had to be varied with each sample and contrast to achieve the best fit however each of the values are within error and this reflects the polydispersity that is also observed in the EM images (Fig. 8). Further evidence of the polydisperse nature of the cubosomes is the high roughness of 49 Å between the cubosome interface and the bulk solvent. As a substantial volume of the cubosomes is water, the nSLD of the cubosome layer changes with solvent contrast as one would expect (Fig. 7) with the lowest cubosome nSLD been in the CMSi contrast with the highest nSLD been the dANX-containing cubosomes in $D_2O$. In this contrast the dANX is be matched out by the $D_2O$ and therefore the volume of PSPhy in the cubosomes can be calculated to be 58%. In a previous study [22], we used combined QCM-D and neutron reflection techniques to study the interaction of PSPhy cubosomes with the POPC model membrane. The QCM-D data also confirm that there was an attractive interaction between the POPC model bilayers and the PSPhy cubosomes. Neutron reflection was able to quantify that around 82% of PSPhy cubosomes were accumulated in the POPC bilayers. Comparing to the current work, the new data show that the PSPhy cubosomes were accumulated to a lesser degree in the POPC/POPS model bilayer than the pure POPC bilayer. The data explain the cell cytotoxicity data shown in Fig. 5 where ANX-PSPhy cubosomes show a smaller reduction in cell viability because ANX reduced cubosome-cell membrane fusion and uptake interactions.

NR data has shown that there is a strong interaction and material exchange between the ANX-PSPhy cubosomes and the model apoptotic lipid bilayer. To study this phenomenon further, we have used Cryo-TEM (Fig. 8) to visualize the intermediate states of the dispersions resulting from material exchange processes when mixing a ratio 1:1 of ANX-PSPhy cubosomes and POPS/POPC vesicles. Fig. 8 indicates that fusion and presumably mixing between POPC/POPS vesicles and cubosomes takes place. We have also

**Table 2**
Properties of bilayer bound ANX-PSPhy cubosomes.

| Component | Thickness/Å | nSLD h-ANX $D_2O$/$\times10^{-6}$ $Å^{-2}$ | nSLD d-ANX $D_2O$/$\times10^{-6}$ $Å^{-2}$ | nSLD d-ANX CMSi/$\times10^{-6}$ $Å^{-2}$ | Roughness/Å | % of bilayer | % PSPhy | % ANX | % solvent |
|---|---|---|---|---|---|---|---|---|---|
| Bilayer properties after cubosome addition | | | | | | | | | |
| Interfacial layer 1 | 27 ± 2 | 1.48 ± 0.51 | 1.79 ± 0.38 | 1.02 ± 0.43 | 6 | 17 | 76 | – | 7 |
| Interfacial layer 2 | 29 ± 6 | 5.72 ± 0.27 | 5.83 ± 0.25 | 4.20 ± 0.46 | 11 | – | 11 | 50 | 39 |

| Contrast | Number of repeats | Repeat length/Å | Average nSLD of repeat/$\times10^{-6}$ $Å^{-2}$ | Amplitude | Phase | Roughness between cubosomes and bulk solvent/Å |
|---|---|---|---|---|---|---|
| Properties of bilayer bound ANX-PSPhy cubosomes | | | | | | |
| h-ANX/$D_2O$ | 89 ± 7 | 46 ± 12 | 2.34 ± 0.46 | 0.58 | 0.96 | 49 |
| d-ANX/$D_2O$ | 84 ± 7 | 45 ± 16 | 2.87 ± 0.49 | 0.22 | 0.76 | 49 |
| d-ANX/CMSi | 92 ± 7 | 41 ± 3 | 1.42 ± 0.06 | 0.14 | 0.008 | 49 |

Please cite this article in press as: Shen H-H, et al., Targeted detection of phosphatidylserine in biomimetic membranes and *in vitro* cell systems using annexin V-containing cubosomes, Biomaterials (2013), http://dx.doi.org/10.1016/j.biomaterials.2013.07.042

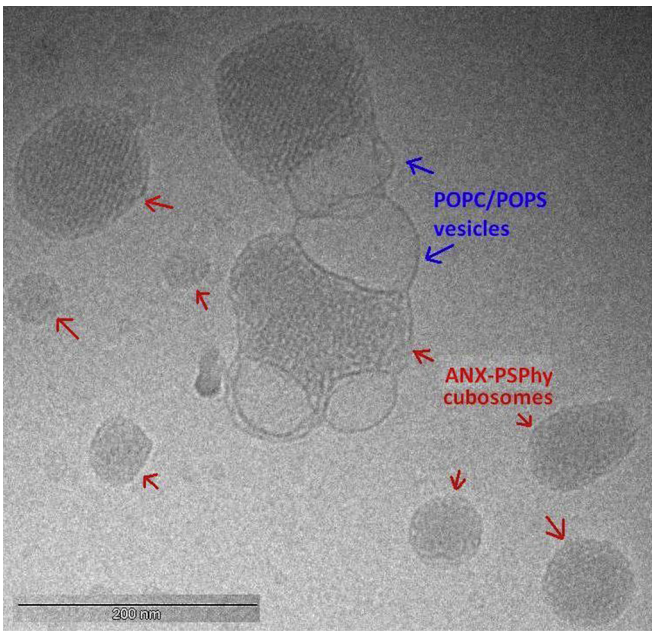


**Fig. 8.** Cryo-TEM image of ANX-PSPhy cubosomes mixed with POPC/POPS (2:1, w:w) vesicles. The red arrows represent the ANX-PSPhy cubosomes. Blue arrows are the vesicles. (For interpretation of the references to colour in this figure legend, the reader is referred to the web version of this article.)

recently observed similar behaviour via synchrotron Small Angle X-ray Scattering studies of pure phytantriol cubosomes interacting with POPC vesicles [21]. Variation in the location and intensity of the Bragg reflections indicates that POPC is migrating from the vesicles into the cubic phase lattice, leading to swelling of the internal nanostructure and a reduction in crystallinity.

Recently some types of Annexin-functionalized nanoparticles have been reported and these nanoparticles were able to image apoptosis *in vitro* [51] and *in vivo* [52]. However the nanoparticles, such as iron oxide nanoparticle [51] and polymeric micelles [52,53] were limited to the application of apoptotic cell detection as a molecular probe. In our study, the ANX-PSPhy cubosomes has not only shown a specific apoptotic cell binding but also found a lipid exchange effect using biophysical approaches. Mulet et al. [54] have also demonstrated that 10 commonly used therapeutic agents, such as progesterone, prednisolone and levofloxacin could be successfully loaded into different types of bicontinuous cubic lyotropic liquid-crystalline dispersed systems, such as phytantriol and monoolein cubosomes, showing superior physical and chemical stability. Our discovery on ANX-PSPhy has therefore demonstrated a great therapeutic potential of apoptotic cell image and drug delivery applications.

## 4. Conclusions

In this work, we have successfully formulated Annexin V-decorated cubosomes (ANX-PSPhy). Both Cryo-TEM and SAXS data show that there is minimal structural rearrangement within the interior of cubosome dispersions due to ANX incorporation suggesting that ANX binds at the PSPhy surface. Using a model membrane system and *in vitro* cell testing, we have shown strong binding between ANX-PSPhy cubosomes and supported apoptotic lipid bilayers and apoptotic cells. We have further used both NR and Cryo-TEM to demonstrate how material exchange occurs between apoptotic membranes and the cubosomes. ANX-PSPhy cubosomes have been shown to discriminate in their binding behaviour between apoptotic and healthy cells. This work has shown that lipid bound proteins can be used to target cubosome systems to biological surfaces *in vitro*. This suggests that similar approaches might be employed to target bicontinuous cubic lyotropic liquid-crystalline dispersed systems *in vivo* with a view to cell targeted imaging or therapeutic delivery.

## Acknowledgements

The authors would like to thank Professor Seamus Martin (Trinity College, Dublin, Ireland) for his kind donation of the pPROEX-Htb_AxV plasmid. The authors acknowledge the facilities, scientific and technical assistance of Monash Micro Imaging, Monash University, Victoria, Australia. The authors are grateful to the Australian Nuclear Science & Technology Organisation (ANSTO), for allocation of beam time for neutron reflectometry measurements, and use of the National Deuteration Facility, which is partially funded by the National Collaborative Research Infrastructure Strategy of the Australian Government, for production of the Annexin V protein used in this study.

## Appendix A. Supplementary data

Supplementary data related to this article can be found at http://dx.doi.org/10.1016/j.biomaterials.2013.07.042.

## References

[1] Kim E, Yang D, Azhdarinia A, Yu DF, Podoloff DA. Imaging and quantification of tumor apoptosis using 99mTc-EC annexin V. Eur J Nucl Med 2001;28:1110.
[2] Lan XL, Zhang YX, An R, Gao ZR, Shen YX. Study of cellular uptake of Tc-99m-HYNIC-annexin V in tumor apoptosis cells. Eur J Nucl Med Mol Imaging 2006;33:S209–10.
[3] Cederholm A, Frostegard J. Annexin A5 in cardiovascular disease and systemic lupus erythematosus. Immunobiology 2005;210:761–8.
[4] Reutelingsperger CPM, vanHeerde WL, Annexin V. the regulator of phosphatidylserine-catalyzed inflammation and coagulation during apoptosis. Cell Mol Life Sci 1997;53:527–32.
[5] van Engeland M, Nieland LJW, Ramaekers FCS, Schutte B, Reutelingsperger CPM. Annexin V-affinity assay: a review on an apoptosis detection system based on phosphatidylserine exposure. Cytometry 1998;31:1–9.
[6] Vermes I, Haanen C, Steffensnakken H, Reutelingsperger C. A novel assay for apoptosis - flow cytometric detection of phosphatidylserine expression on early apoptotic cells using fluorescein-labeled Annexin-V. J Immunol Methods 1995;184:39–51.
[7] Vanoers MHJ, Reutelingsperger CPM, Kuyten GAM, Vondemborne AEGK, Koopman G. Annexin-V for flow cytometric detection of phosphatidylserine expression on B-cells undergoing apoptosis. Blood 1994;84:A291.
[8] Buzhynskyy N, Golczak M, Lai-Kee-Him J, Lambert O, Tessier B, Gounou C, et al. Annexin-A6 presents two modes of association with phospholipid membranes. A combined QCM-D, AFM and cryo-TEM study. J Struct Biol 2009;168:107–16.
[9] Cordeiro MF, Guo L, Luong V, Harding G, Wang W, Jones HE, et al. Real-time imaging of single nerve cell apoptosis in retinal neurodegeneration. Proc Natl Acad Sci U S A 2004;101:13352–6.
[10] Cao W, Huang JS, Wu JY, Cao GX, He Y, Hu D, et al. Study of Tc-99m-annexin V uptake in apoptotic cell models of Parkinson's disease. Nucl Med Commun 2007;28:895–901.
[11] Angelova A, Angejov B, Lesieur S, Mutafchieva R, Ollivon M, Bourgaux C, et al. Dynamic control of nanofluidic channels in protein drug delivery vehicles. J Drug Deliv Sci Technol 2008;18:41–5.
[12] Boyd BJ, Whittaker DV, Khoo SM, Davey G. Hexosomes formed from glycerate surfactants – formulation as a colloidal carrier for irinotecan. Int J Pharm 2006;318:154–62.
[13] Nguyen TH, Hanley T, Porter CJH, Boyd BJ. Nanostructured liquid crystalline particles provide long duration sustained-release effect for a poorly water soluble drug after oral administration. J Control Release 2011;153:180–6.
[14] Conn CE, Darmanin C, Mulet X, Hawley A, Drummond CJ. Effect of lipid architecture on cubic phase susceptibility to crystallisation screens. Soft Matter 2012;8:6884–96.
[15] Conn CE, Drummond CJ. Nanostructured bicontinuous cubic lipid self-assembly materials as matrices for protein encapsulation. Soft Matter 2013;9:3449–64.
[16] Yaghmur A, Glatter O. Characterization and potential applications of nanostructured aqueous dispersions. Adv Colloid Interface Sci 2009;147-48:333–42.

[17] Amar-Yuli I, Wachtel E, Ben Shoshan E, Danino D, Aserin A, Garti N. Hexosome and hexagonal phases mediated by hydration and polymeric stabilizer. Langmuir 2007;23:3637–45.
[18] Dong YD, Larson I, Hanley T, Boyd BJ. Bulk and dispersed aqueous phase behavior of phytantriol: effect of vitamin E acetate and F127 polymer on liquid crystal nanostructure. Langmuir 2006;22:9512–8.
[19] Barauskas J, Landh T. Phase behavior of the phytantriol/water system. Langmuir 2003;19:9562–5.
[20] Rizwan SB, Dong YD, Boyd BJ, Rades T, Hook S. Characterisation of bicontinuous cubic liquid crystalline systems of phytantriol and water using cryo field emission scanning electron microscopy (cryo FESEM). Micron 2007;38:478–85.
[21] Shen HH, Crowston JG, Huber F, Saubern S, McLean KM, Hartley PG. The influence of dipalmitoyl phosphatidylserine on phase behaviour of and cellular response to lyotropic liquid crystalline dispersions. Biomaterials 2010;31:9473–81.
[22] Shen HH, Hartley PG, James M, Nelson A, Defendi H, McLean KM. The interaction of cubosomes with supported phospholipid bilayers using neutron reflectometry and QCM-D. Soft Matter 2011;7:8041–9.
[23] Logue SE, Elgendy M, Martin SJ. Expression, purification and use of recombinant annexin V for the detection of apoptotic cells. Nat Protoc 2009;4:1383–95.
[24] Middelberg APJ, Oneill BK, Bogle IDL, Snoswell MA. A novel technique for the measurement of disruption in high-pressure homogenization – studies on *Escherichia coli* containing recombinant inclusion-bodies. Biotechnol Bioeng 1991;38:363–70.
[25] Chen X, Wilde KL, Wang H, Lake V, Holden PJ, Middelberg APJ, et al. High yield expression and efficient purification of deuterated human protein galectin-2. Food Bioprod Process 2012;90:563–72.
[26] Mosmann T. Rapid colorimetric assay for cellular growth and survivals: application to proliferation and cytotoxicity assays. J Immunol Methods 1983;65:55–63.
[27] James M, Nelson A, Brule A, Schulz JC. Platypus: a time-of-flight neutron reflectometer at Australia's new research reactor. J Neutron Res 2006;14:91–108.
[28] James M, Nelson A, Holt SA, Saerbeck T, Hamilton WA, Klose F. The multipurpose time-of-flight neutron reflectometer "Platypus" at Australia's OPAL reactor. Nucl Instrum Meth A 2011;632:112–23.
[29] Nelson A. Motofit – integrating neutron reflectometry acquisition, reduction and analysis into one, easy to use, package. J Phys Conf Ser 2010;251:012094.
[30] Nelson A. Co-refinement of multiple-contrast neutron/X-ray reflectivity data using MOTOFIT. J Appl Crystallogr 2006;39:273–6.
[31] Born M, Wolf E. Principle opt. 7th ed.; 1980.
[32] Thomas RK, Lu JR, Penfold J. Applications of neutron reflectometry in surface science. Surf Layers 1994;154:153–62.
[33] Vandoolaeghe P, Rennie AR, Campbell RA, Nylander T. Neutron reflectivity studies of the interaction of cubic-phase nanoparticles with phospholipid bilayers of different coverage. Langmuir 2008;25:4009–20.
[34] Vandoolaeghe P, Campbell RA, Rennie AR, Nylander T. Adsorption of intact cubic liquid crystalline nanoparticles on hydrophilic surfaces: lateral organization, interfacial stability, layer structure, and interaction mechanism. J Phys Chem C 2009;113:4483–94.
[35] Samani MB, Whitten P, Spinks G, Cook C. Viscoelastic study of conducting polymers using quartz crystal microbalance. Smart Mater Struct 2006;6168:616810–27.
[36] Concha NO, Head JF, Kaetzel MA, Dedman JR, Seaton BA. Annexin-V forms calcium-dependent trimeric units on phospholipid-vesicles. FEBS Lett 1992;314:159–62.
[37] Hofmann A, Ruvinov S, Hess S, Schantz R, Delmer DP, Wlodawer A. Plant annexins form calcium-independent oligomers in solution. Protein Sci 2002;11:2033–40.
[38] Mo Y, Campos B, Mealy TR, Commodore L, Head JF, Dedman JR, et al. Interfacial basic cluster in annexin V couples phospholipid binding and trimer formation on membrane surfaces. J Biol Chem 2003;278:2437–43.
[39] Sagalowicz L, Michel M, Adrian M, Frossard P, Rouvet M, Watzke HJ, et al. Crystallography of dispersed liquid crystalline phases studded by cryo-transmission on electron microscopy. J Microsc 2006;221:110–21.
[40] Yaghmur A, de Campo L, Sagalowicz L, Leser ME, Glatter O. Control of the internal structure of MLO-based isasomes by the addition of diglycerol monooleate and soybean phosphatidylcholine. Langmuir 2006;22:9919–27.
[41] Wadsten-Hindrichsen P, Bender J, Unga J, Engstrom S. Aqueous self-assembly of phytantriol in ternary systems: effect of monoolein, distearoylphosphatidylglycerol and three water-miscible solvents. J Colloid Interface Sci 2007;315:701–13.
[42] Conn CE, Mulet X, Moghaddam MJ, Darmanin C, Waddington LJ, Sagnella SM, et al. Enhanced uptake of an integral membrane protein, the dopamine D2L receptor, by cubic nanostructured lipid nanoparticles doped with Ni(II) chelated EDTA amphiphiles. Soft Matter 2011;7:567–78.
[43] Richter R, Mukhopadhyay A, Brisson A. Pathways of lipid vesicle deposition on solid surfaces: a combined QCM-D and AFM study. Biophys J 2003;85:3035–47.
[44] Richter RP, Brisson AR. Following the formation of supported lipid bilayers on mica: a study combining AFM, QCM-D, and ellipsometry. Biophys J 2005;88:3422–33.
[45] Boland MP, Hatty CR, Separovic F, Hill AF, Tew DJ, Barnham KJ, et al. Anionic phospholipid interactions of the prion protein N terminus are minimally perturbing and not driven solely by the octapeptide repeat domain. J Biol Chem 2010;285:32282–92.
[46] Caruso F, Serizawa T, Furlong DN, Okahata Y. Quartz-crystal microbalance and surface-plasmon resonance study of surfactant adsorption onto gold and chromium-oxide surfaces. Langmuir 1995;11:1546–52.
[47] Zhang XD, Gillespie SK, Hersey P. Staurosporine induces apoptosis of melanoma by both caspase-dependent and -independent apoptotic pathways. Mol Cancer Ther 2004;3:187–97.
[48] Esposito E, Cortesi R, Drechsler M, Paccamiccio L, Mariani P, Contado C, et al. Cubosome dispersions as delivery systems for percutaneous administration of indomethacin. Pharm Res 2005;22:2163–73.
[49] Vandoolaeghe P, Rennie AR, Campbell RA, Thomas RK, Hook F, Fragneto G, et al. Adsorption of cubic liquid crystalline nanoparticles on model membranes. Soft Matter 2008;4:2267–77.
[50] Chiu SW, Jakobsson E, Subramaniam S, Scott HL. Combined monte carlo and molecular dynamics simulation of fully hydrated dioleyl and palmitoyl-oleyl phosphatidylcholine lipid bilayers. Biophys J 1999;77:2462–9.
[51] Li Z-F, Liu L, Tian W, Teng G-J, Zhang Y, Ge Y-Q, et al. MRI observation of apoptotic cells using superparamagnetic iron oxide nanoparticles labeled annexin V in vitro. Chin J Med Imaging Technol 2009;25:734–9.
[52] Zhang R, Lu W, Wen X, Huang M, Zhou M, Liang D, et al. Annexin A5-conjugated polymeric micelles for dual SPECT and optical detection of apoptosis. J Nucl Med 2011;52:958–64.
[53] Zhang R, Huang M, Zhou M, Wen X, Huang Q, Li C. Annexin A5-functionalized nanoparticle for multimodal imaging of cell death. Mol Imaging 2013;12:182–90.
[54] Drummond CJ, Mulet X, Kennedy DF, Conn CE, Hawley A. High throughput preparation and characterisation of amphiphilic nanostructured nanoparticulate drug delivery vehicles. Int J Pharm 2010;395:290–7.

Please cite this article in press as: Shen H-H, et al., Targeted detection of phosphatidylserine in biomimetic membranes and *in vitro* cell systems using annexin V-containing cubosomes, Biomaterials (2013), http://dx.doi.org/10.1016/j.biomaterials.2013.07.042